Journal of Power Sources 264 (2014) 299–310

Contents lists available at ScienceDirect

Journal of Power Sources

journal homepage: www.elsevier.com/locate/jpowsour

Grain boundary driven capacity fade/hysteresis abated in composite cathode material for lithium-ion batteries/pouch cell

P. Manikandan, P. Periasamy [1], R. Jagannathan*

Lithium Batteries – Electrochemical Power Sources Division and Functional Materials Division, CSIR – Central Electrochemical Research Institute, Karaikudi-630 006, Tamilnadu, India

HIGHLIGHTS

- Charge transport (Li^+, e^-) across edges of faceted particles costs much energy.
- Smooth surfaced, fade abated composite cathode particles.
- Electrochemical hysteresis (irreversibility) predicted through CV.
- Li *vs* LNMC-LNM cell delivered discharge capacity of 194 mAh g^{-1} ($\Delta Q_{Li} = -11\%$).
- W-weaving style Li-ion pouch cell fabricated with composite cathode/anode.

GRAPHICAL ABSTRACT

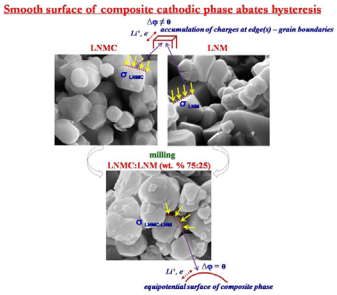

ARTICLE INFO

Article history:
Received 6 February 2014
Received in revised form
8 April 2014
Accepted 14 April 2014
Available online 30 April 2014

Keywords:
Mixed hydroxy-carbonate
Composite cathode material
Irreversible capacity-hysteresis
Grain boundary
Lithium-ion pouch cell

ABSTRACT

The composite cathode material $LiNi_{1/3}Mn_{1/3}Co_{1/3}O_2$:$LiNi_{0.5}Mn_{0.5}O_2$ (wt. % 75:25) comprising the blend of well characterized $LiNi_{1/3}Mn_{1/3}Co_{1/3}O_2$ and $LiNi_{0.5}Mn_{0.5}O_2$ materials has been synthesized through a facile thermolysis employing mixed hydroxy-carbonate precursor. This composite cathode material yielded impressive charge–discharge profile with a capacity of 213/194 mAh g^{-1} at 0.1 C and amazing coulombic efficiency of 99.4% at 50th cycle. Notwithstanding impressive initial charge–discharge capacity of the individual LNMC phase 224/187 mAh g^{-1} attributed to sharp edges of the cathode particles showed large irreversible capacity-hysteresis. Near absence of irreversible capacity observed upon discharging the composite cathode material can be attributed to milled/smoothened cathode particles of the composite cathode material offering little scope for energy loss in contrast to sharp edge-grain boundary induced irreversibility-hysteresis seen in the individual phases ($LiNi_{1/3}Mn_{1/3}Co_{1/3}O_2$ and $LiNi_{0.5}Mn_{0.5}O_2$). The application scope of the high performance composite cathode material has been widened in conjunction with graphitic alloy anode ($G_{0.65}Ni_{0.05}Ti_{0.15}Sn_{0.15}$) material as demonstrated with the fabrication of W-weaving style design of Li-ion pouch cell (~500 mAh) at moderate loads 0.12 Wh, 1.1 Wh.

1. Introduction

The dawn of 90s witnessed renaissance in electrochemical power sources with the advent of first commercial rechargeable Li-ion batteries introduced by Sony. Li-ion batteries offering high energy storage and excellent rechargeability are considered as one of the most important energy storage system for multifarious applications

* Corresponding author. Tel.: +91 9487167780; fax: +91 4565227713.
E-mail addresses: periasamylibatt@gmail.com (P. Periasamy), jaganr_57@yahoo.co.in, jags57_99@yahoo.com (R. Jagannathan).
[1] Tel.: +91 4565241421; fax: +91 4565227713.

http://dx.doi.org/10.1016/j.jpowsour.2014.04.064
0378-7753/

[1–4]. In the design of Li-ion batteries, the choice of the cathode system holds the key in determining the electrochemical performance. Especially the chemical constituents and allied materials properties are very crucial which eventually determine the key electrochemical parameters *viz.*, good cyclic stability and stable discharge voltage. The first entrant of the cathode system, the layered $LiCoO_2$ seem to meet these important requirements of good cyclic stability and stable discharge voltage [5]. However, this cathode system suffers from inherent disadvantages of being toxic, expensive, low practical capacity (0.5 Li) added with more challenges such as safety, charging limitation not exceeding 4.2 V owing to structural degradation problem curtailing the application scope in particular for electric vehicles [6–8]. Notwithstanding these challenging issues ruling against the use of layered $LiCoO_2$ cathode for applications, the cathode system still reigns the lithium battery industry in terms of easy synthesis, cyclic stability and charge–discharge stability.

These challenges serve as motivation in the search for alternative cathode system such as $LiNi_{1/3}Mn_{1/3}Co_{1/3}O_2$ and $LiNi_{0.5}Mn_{0.5}O_2$ (LNMC and LNM) layered materials and so on. The LNMC [9,10] and LNM [11,12] cathode systems have an edge over conventional layered oxide cathode system being presently used in terms of cell voltage, impressive capacity coupled with structural stability and cycling performance. In view of the application potential of this system, there are numerous trials reporting on syntheses of LNMC and LNM such as solid-state [11,13,14], hydroxide co-precipitation [15–17] and combustion [18,19] methods yielding cathode particles having different morphologies. Because, these layered materials still have further scope for improvement in capacity we are motivated to explore synthesis strategies ensuring homogenous distribution of cations through atomic scale-mixing of Ni, Co, and Mn ions [20] so that still impressive electrochemical performance can be expected. Traditionally hydroxide co-precipitation method is employed for the synthesis of LNMC and LNM cathode materials. However, this method involving synthesis under basic conditions pH $>$ 7 has the inherent drawback of entailing in gelatinous precipitate essentially comprising hydroxide phase eventually hampering the dispersion of target particles. This can be overcome with the co-occurrence of carbonaceous phase along with hydroxide phase [21]. Mixed hydroxy-carbonate (MHC) synthesis under near neutral condition is more advantageous over basic conditions because the former results in more dispersible homogeneous particles of the target phase [21]. Eventually it turns out that toxic free MHC [$(Ni_{1/3}Mn_{1/3}Co_{1/3})_2(OH)_2CO_3$, $(Ni_{0.5}Mn_{0.5})_2(OH)_2CO_3$] precursors can also lead to oxidic cathode products having high dispersibility [21] owing to evolution of non-toxic gases *viz.*, water, carbon dioxide upon decomposition.

In order to achieve higher capacity, good thermal stability and abated capacity fade, the important attributes of cathode system realized through a new strategy involving physical mixture of moderate composite cathode materials having two different types of insertion materials [22–32]. Obviously, synthesizing a composite cathode through the blend of selected cathodic phases using a mixer-ball mill is well established now. There are many reports on several types of composite cathode materials *viz.*, the mixture of LNMC and LNM layered materials [23,24]; spinel type $LiMn_2O_4$ and layered $LiMO_2$ cathode materials [25–30] also olivine type $LiMPO_4$ and layered $LiMO_2$ materials [31,32]. It is well known that the LNMC compound yields higher capacity while the LNM compound gives good thermal stability [23]. Hence, it is reasonable to expect that the composite of these cathode materials can offer both high capacity and good thermal stability [23] addressing safety issue at higher voltage ($>$4.2 V). These distinguishing features make the composite cathode systems very attractive for eventual application in battery designing. Normally in the fabrication of composite cathode, LNMC phase constitutes major portion ($\geq$70 wt. %) to facilitate higher capacity.

The scope of present investigation focuses on achieving phase purity, structural properties, morphology and electrochemical performance of the composite cathode (CC) $LiNi_{1/3}Mn_{1/3}Co_{1/3}O_2$:$LiNi_{0.5}Mn_{0.5}O_2$ (LNMC:LNM ↔ CC) materials. Another major daunting task which concerns in the design of Li-ion batteries is unduly excessive weight of metallic cell casings which when stacked in large numbers limit the scope for large-scale application. However, the issue of excessive weight of the casings can be overcome through alternative design based on pouches made of aluminum foil [33]. Taking stock of this scenario in the design of Li-ion batteries, we present and discuss our results on high voltage

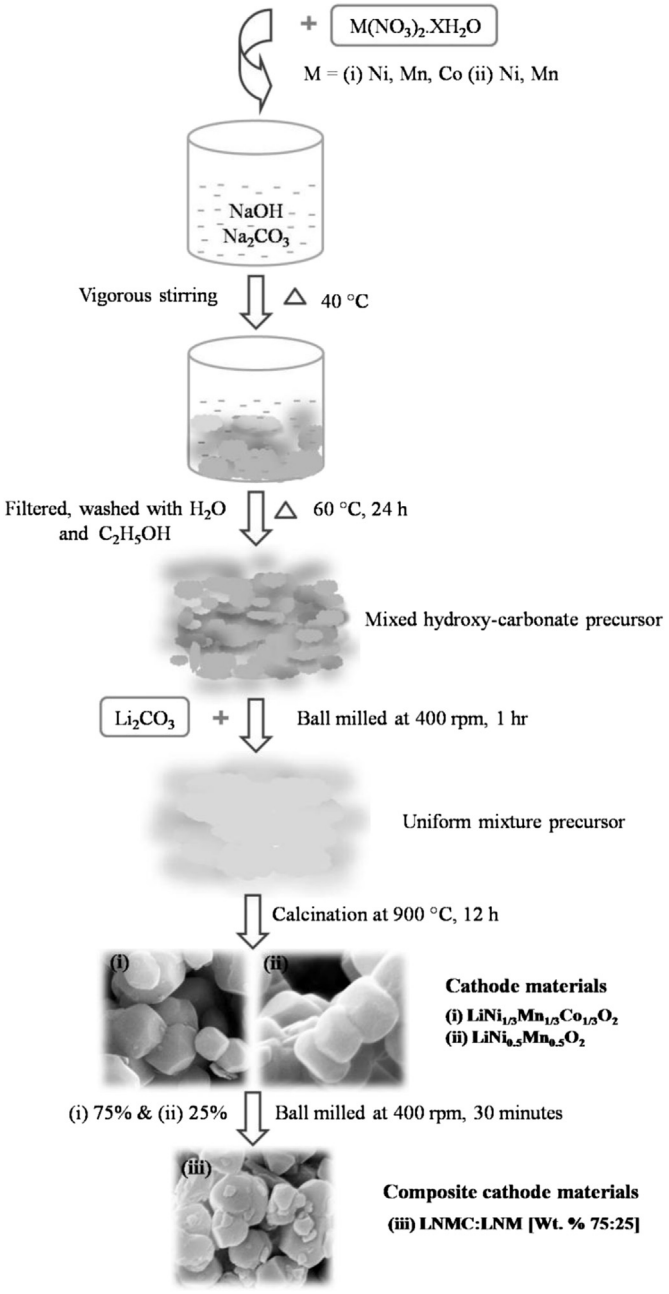

Fig. 1. Schematics on the synthesis of composite cathode material (75%LNMC:25% LNM ↔ CC-2) using facile non toxic MHC precursor.

energy storage system *viz.*, Li-ion pouch cell fabricated with the advanced graphitic alloy anode *vs* CC-2 composite cathode materials for the Li-ion batteries.

2. Experimental aspects

2.1. Synthesis of LNMC:LNM composite cathode materials

In this work the cathode material has been synthesized through a facile route comprising three steps with (i) synthesis of MHC precursor underlying co-precipitation of Ni, Mn and Co ions followed by (ii) MHC precursor yielding the oxidic individual cathodic products (iii) preparation of LNMC:LNM composite cathode by mixing two different types of layered compounds (LNMC and LNM phases) as schematized in Fig. 1. The synthesis sequence are: $(Ni_{1/3}Mn_{1/3}Co_{1/3})_2(OH)_2CO_3$ precursor was synthesized using stoichiometric aqueous solutions of $Ni(NO_3)_2\cdot 6H_2O$, $Mn(NO_3)_2\cdot 4H_2O$ and $Co(NO_3)_2\cdot 6H_2O$ (Merck AR grade). This mixed solution was slowly added to a mixture of NaOH (2 mol) and Na_2CO_3 (1 mol) aqueous solution at 40 °C under lab ambient conditions (air atmosphere) through stirring until complete precipitation appearing as green dark brownish gelatinous precipitate, which was filtered, washed using distilled water and ethanol followed by drying at 60 °C for 24 h resulting in the MHC precursor. Then, stoichiometric amounts of this MHC precursor and Li_2CO_3 were homogenized and ground well for 1 h using FRITSCH pulverisette 7 instrument at 400 rpm. After the homogenization step, this blend was calcined 900 °C for 12 h to get oxidic LNMC cathodic phase. Under similar conditions, the other phase LNM also obtained. Upon calcination, the thermal decomposition of the starting materials blend of MHC and Li_2CO_3 can be visualized through the following reactions (1) and (2):

$$Li_2CO_3 + \left(Ni_{1/3}Mn_{1/3}Co_{1/3}\right)_2(OH)_2CO_3 + 1/2O_2 \xrightarrow{\Delta(900\,^\circ C)} 2LiNi_{1/3}Mn_{1/3}Co_{1/3}O_2 + 2CO_2\uparrow + H_2O\uparrow \quad (1)$$

$$Li_2CO_3 + (Ni_{0.5}Mn_{0.5})_2(OH)_2CO_3 + 1/2O_2 \xrightarrow{\Delta(900\,^\circ C)} 2LiNi_{0.5}Mn_{0.5}O_2 + 2CO_2\uparrow + H_2O\uparrow \quad (2)$$

In the present investigations, compositions by varying the relative wt. % of LNMC and LNM phases respectively in the range of 70–80 and 30–20 have been synthesized. We present the performance profiles of three sets of pre optimized composite cathodes having compositions relative wt. % of 70:30 (CC-1), 75:25 (CC-2) and 80:20 (CC-3) as representative examples. In this work, these composite cathode materials were blended through gentle milling at 400 rpm for 30 min as depicted in Fig. 1. In order to ascertain the role of blending/milling the individual constituent LNMC, LMN were also subjected to similar milling treatments.

Turning to describe the preparation of the graphitic alloy anode: graphite (G), $G_{0.85}Sn_{0.15}$, $G_{0.70}Ti_{0.15}Sn_{0.15}$ and $G_{0.65}Ni_{0.05}Ti_{0.15}Sn_{0.15}$ were synthesized through high energy ball milling using graphite (<100 μm, 99.5%, S D Fine), Sn (−100 mesh, 99.85%, metal basis, Alfa Aesar), Ti (98.5%, Himedia) and Ni (100 mesh, 99.5%, S D Fine) powders. Required amount (weight %) of metal powders were mixed together and milled for 30 h (Ar atmosphere) using FRITSCH pulverisette 7 pulverizer at 500 rpm followed by heating at 900 °C for 5 h in Ar atmosphere.

2.2. Characterization

Chemical purity of the as-prepared samples *viz.*, LNMC, LNM individual phases and composite cathode material (LNMC:LNM) has been ascertained through powder X-ray diffraction (XRD) studies using a Bruker D8 Advance X-ray diffractometer with a Cu Kα X-ray source ($\lambda = 1.5418$ Å, with corundum Al_2O_3 as the internal standard) and the measurements were recorded with 2θ range 10–80°, and the XRD data have been refined using a least squares data refinement program. Various functional groups present in the MHC precursors and also in the cathode materials have been analyzed using FT-IR spectra (BRUKER Optik GmbH MODEL TENSOR 27 FT-IR spectrometer with a detector RT DLaTGS) using a KBr pellet in the range 400–4000 cm^{-1}. Particle morphologies of the precursor, LNMC, LNM and LNMC:LNM cathode phase/material were analyzed through field-emission scanning electron microscopy (FE-SEM) MODEL ZEISS SUPRA™ 55VP.

Turning to electrochemical characterization, cyclic voltammograms (CV) were recorded at several scan rate of 0.1–1 mV s^{-1} in the voltage range 2.5–4.8 V under CR2032 cell configuration using VMP3Z (Biologica) Multi-Channel Potentiostat/Galvanostat electrochemical workstation. Electrochemical impedance spectroscopy (EIS) analyses was carried out for CR2032 configuration cells using VMP3Z (Biologica) Multi-Channel Potentiostat/Galvanostat electrochemical workstation over a frequency range 100 kHz to 10 mHz. Galvanostatic charge–discharge studies were made using Arbin multichannel cycler instrument (BT2000). Coin cells were assembled using lithium foil (thickness: 0.75 mm) as anode and as-prepared LNMC, LNM, LNMC:LNM materials coated on Al foil as cathode. Notably, Li-ion pouch cell with Celgard® 2340 separator (stacking in W-weaving style) has been fabricated using six (four double-side and two single-side coated) negative electrodes and five (double-side) positive electrodes inside a laminated pouch. In this trial, active materials of the negative and positive electrodes used were $G_{0.65}Ni_{0.05}Ti_{0.15}Sn_{0.15}$ and CC-2, respectively along with 1 M solution of $LiPF_6$ in 1:1 (v/v) EC–DMC mixture was used as the electrolyte.

In the fabrication of Li-ion pouch cell, crucial design parameters are electrode area (double side) and electrode thickness (with current collector) of the negative/positive electrodes which were respectively 5 × 5 cm^2 and 147/142 μm using $G_{0.65}Ni_{0.05}Ti_{0.15}Sn_{0.15}$ and CC-2 electrode materials. Furthermore the cathode was fabricated using doctor blade-coating slurry of 80% CC-2, 15% SP-carbon (Timcal) and 5% PVdF in NMP coated over aluminum foil (15 μm). The anode was fabricated using 80% $G_{0.65}Ni_{0.05}Ti_{0.15}Sn_{0.15}$, 15% SP-carbon (Timcal) and 5% PVdF in NMP slurry coated over copper foil (9 μm) and dried at 85 °C for 12 h in a vacuum oven. The area, thickness and weight of the negative/positive electrodes were 1.54 cm^2, 78/75 μm and 5.6/12.7 mg (active material, 80%) under CR2032 cell configuration. Both coin and pouch cells were assembled in an argon-filled glove box (mBRAUN MB200G) with oxygen and moisture levels less than 0.1 ppm. Cell performance of the coin cells were evaluated through charge–discharge studies in the range of 2.5 and 4.6 V at 0.1 C, 1 C, 2 C, 3 C and 5 C rates at room temperature. The performance of the fabricated pouch cell has been investigated through charge–discharge studies and also further used in demonstration kits *viz.*, operation of LED array, electronic toy-car.

3. Results and discussion

The procedure adopted for the synthesis of both LNMC and LNM phases has been essentially based on MHC method. It is known that when a composite of these two phases are used for Li-ion battery applications, safety issue can be adequately addressed [23]. Accordingly, a thoroughly homogenized blend of LNMC and LNM phases was obtained through ball milling of LNMC, LNM phases respectively taken in the weight % of 75:25 (3:1 ratio) with relevant details schematized in Fig. 1. This synthesis sequence has several advantages *viz.*, facile toxic free route, batch-size up scalability

(~50 g in lab-scale) and so on. Furthermore, this facile route requires only shorter milling time (~1 h) coupled with remarkable electrochemical performance as would be elaborated subsequently in this report.

3.1. Crystallographic parameters through XRD

Concerning the synthesis of LNMC [10,34] and LNM [12] phases, the temperature and duration of milling seem to be very crucial in determining various parameters influencing electrochemical performance *viz.*, highly crystalline particles, least cation mixing and perfect hexagonal ordering coupled with pronounced lithium (de) intercalation processes. Accordingly, the synthesis conditions for the LNMC and LNM phases have been optimized at 900 °C for 12 h and the corresponding XRD patterns along with composite cathode material as depicted in Fig. 2. Obviously, XRD patterns of the individual LNMC and LNM as well the composite cathode material are consistent with JCPDS# 01-087-1564 indexable under space group *R*3*m* adopting hexagonal α-$NaFeO_2$ type structure. Notwithstanding perfect matching of these XRD lines, the pattern corresponding to the composite cathode material reveals faint satellite profile at (101) and (104) planes as indicated using * mark, which can be attributed to broader line width of LNM phase. Furthermore, sharp splitting pairs corresponding to (006), (102) and (108), (110) planes observed for these systems are a clear indicator of perfect hexagonal ordering with good crystallinity (Fig. 2). Least squares refined crystallographic cell parameters and the cell-volume deduced for these samples show good agreement (Table 1). In particular the relative intensity ratio of $I_{(003)}/I_{(104)}$ is very important that when it is higher than 1.2 would yield favorable conditions such as least cation mixing owing to perfect hexagonal ordering coupled with pronounced lithium (de)intercalation processes [13]. Importantly, it should borne in mind that this XRD line intensity ratio for all these cathode phase/material show an impressive value in the range of 1.7–2.4 which in turns to suggests least cation mixing between Li and Ni ions in the hexagonal structure, a property most preferred for superior performance of the cathodes [35]. Also, low value for $R = (I_{006} + I_{102})/I_{101}$ corresponding to the LNMC and CC-2 cathode materials confirms again higher hexagonal ordering for the impressive electrochemical performance [35,36].

Table 1
Comparison of crystallographic refined cell parameters and XRD line intensity ratio of cathode phase/material *viz.*, LNMC, LNM, and CC-2.

Sample	*a* (Å)	*c* (Å)	*c*/*a*	*V* (Å)^3	I_{003}/I_{104}	$R = I_{006} + I_{102}/I_{101}$
NMC	2.8512	14.1507	4.9630	99.62	1.7398	0.4577
LNM	2.8810	14.2410	4.9430	102.37	2.0530	0.8019
CC-2	2.8597	14.2134	4.9702	100.66	2.4371	0.4971

3.2. Insights on functional groups of cathode phase/material

FT-IR spectral data on these inorganic $(Ni_{1/3}Mn_{1/3}Co_{1/3})_2(OH)_2CO_3$, $(Ni_{0.5}Mn_{0.5})_2(OH)_2CO_3$ precursors, LNMC, LNM and CC-2 cathode phase/material (Fig. 3) yield reliable information on various functional groups present and their modes of interaction/vibration. The precursor material exhibits characteristic frequencies corresponding to stretching ν(O–H) at 3400 cm^{-1} arising from the stretching vibration ν(O–H) of H_2O molecule and also due to hydroxy groups in the mixed hydroxy-carbonate precursors as reported by others [21]. As can be seen in Fig. 3, the presence of δ(O–H) bending vibration of water vapor at 1634 cm^{-1} may suggest trace amounts of absorption water in the electrode materials [37]. Also in this precursor material, carbonate group signatures revealed through four modes of vibrations *viz.*, $\nu_1(CO_3^{2-}$ symmetric stretching vibration) at 1060 cm^{-1}, $\nu_2(CO_3^{2-}$ out-of-plane deformation vibration) at 861 cm^{-1}, $\nu_3(CO_3^{2-}$ asymmetric stretching vibration) at 1420 cm^{-1} and $\nu_4(CO_3^{2-}$ in-plane deformation vibration) at 734 cm^{-1} are consistent with reports on carbonate group FT-IR data [21,38]. These data reliably confirm the formation of mixed hydroxy-carbonate *viz.*, $(Ni_{1/3}Mn_{1/3}Co_{1/3})_2(OH)_2CO_3$ (blue line), $(Ni_{0.5}Mn_{0.5})_2(OH)_2CO_3$ (green line) precursors used for LNMC and LNM synthesis. Moving over to FT-IR spectral data for the LNMC (red line), LNM (dark cyan line) and CC-2 (brown line) cathode phase/material (Fig. 3), it can be seen that hydroxy and carbonate groups are totally absent owing to the complete thermal decomposition of the precursor materials. However we observe a clear proof for the occurrence of metal oxygen M–O bond vibrations assignable under different characteristic modes: asymmetric stretching $\nu(MO_6)$ at 597 cm^{-1} [39] and bending vibrations δ(O–M–O) at 543 cm^{-1} [40] thereby confirming the chemical integrity

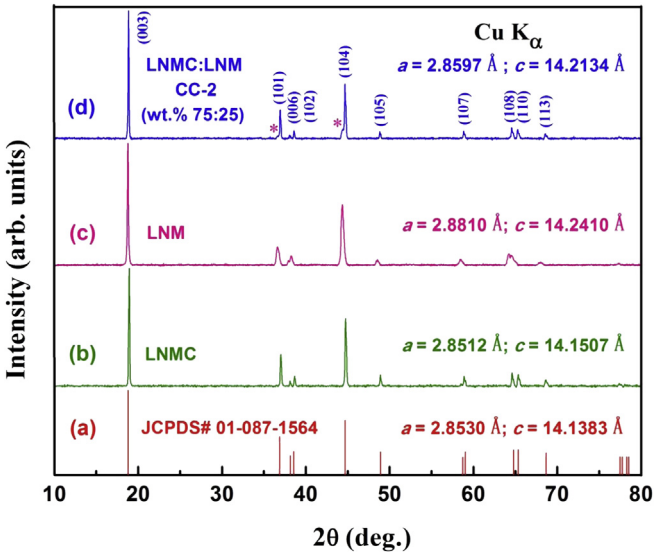

Fig. 2. Powder X-ray diffraction patterns of cathode phases: (a) JCPDS# 01-087-1564 standard, (b) LMNC, (c) LNM synthesized at 900 °C for 12 h using MHC precursor and (d) CC-2 composite cathode materials.

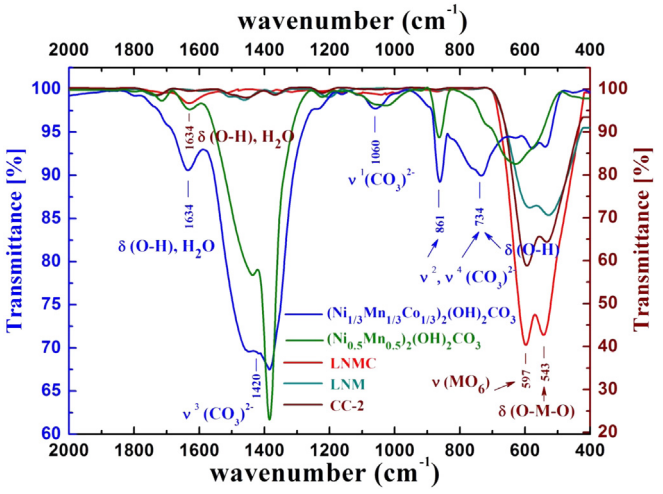

Fig. 3. FT-IR spectra of such as MHC $(Ni_{1/3}Mn_{1/3}Co_{1/3})_2(OH)_2CO_3$ (blue line), $(Ni_{0.5}Mn_{0.5})_2(OH)_2CO_3$ (green line) precursor, LNMC (red line), LNM (dark cyan line) and CC-2 (brown line) cathode phase/material. (For interpretation of the references to color in this figure legend, the reader is referred to the web version of this article.)

of the intended LNMC, LNM and CC-2 cathode phase/material as depicted in Fig. 3.

3.3. Morphology of precursors and cathode phase/material using FE-SEM

Particle size and morphology of the cathode phase/material hold the key in achieving good electrochemical performance for eventual Li-ion batteries [15]. Because precise analysis and appraisal on the particle morphology are crucial, a more powerful and reliable microscopic analytical method based on FE-SEM has been employed in this investigation. Invariably the morphology of precursors for both LNMC and LNM phases adopts spongy, floral growth comprising minute lamellar flakes (~30 nm) as depicted in Fig. 4a, b. This morphology stemming from MHC precursor phase is quite characteristic of a gelatinous precipitate obtained through wet chemical method. Fine particles of the MHC precursors obtained after drying (60 °C for 24 h) are favorable for the synthesis of cathode particles of desirable morphology facilitated through homogeneous admixture with the Li_2CO_3. Furthermore, upon thermolysis this mixture generates H_2O and CO_2 gases which might aid to obtain well dispersed cathode particles [21]. It turns out that the particle features of LNMC and LNM phases thus synthesized seem to resemble each other in terms of both particle morphology and size (~200 nm). The distinguishing trait of the cathode particles adopting polyhedral morphology which are faceted with well defined phases demarcated through blunted edges (highlighted using yellow colored circles and arrows in Fig. 4c, d). Results of the present investigation have shown that the composite cathode material yields higher capacity coupled with good capacity retention. In order to understand the origin of the enhancement of the composite phase, detailed examination of its morphology merits attention. Accordingly, the morphology of the composite cathode material has been examined thoroughly focusing different directions (Fig. 4e, f). As could be seen from the micrographs, particles of the composite cathode material are essentially made of smoothened polyhedral particles. The edge smoothening observed in the composite cathode particles can be rationalized in terms of gentle milling smearing out the edges of the particles without much comminuting in size.

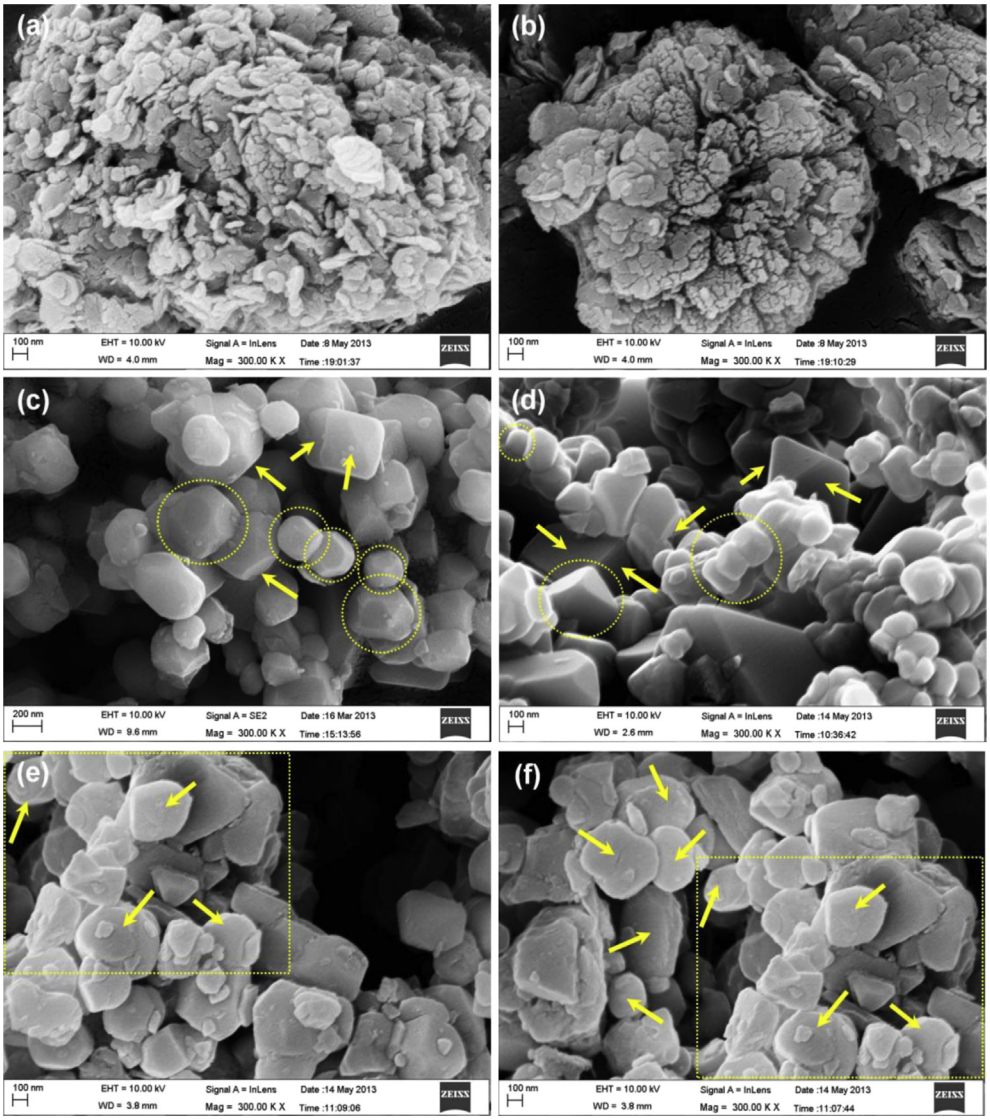

Fig. 4. Morphological investigation using FE-SEM for the MHC precursors and cathode phase/material. Spongy morphology for MHC precursors (a) $(Ni_{1/3}Mn_{1/3}Co_{1/3})_2(OH)_2CO_3$ and (b) $(Ni_{0.5}Mn_{0.5})_2(OH)_2CO_3$; well dispersed polyhedral particles with regular faceted edges (c) LNMC and (d) LNM phases; (e,f) CC-2 composite cathodic particles with smooth surface under different directions. All images were recorded at 300 K × magnifications respectively.

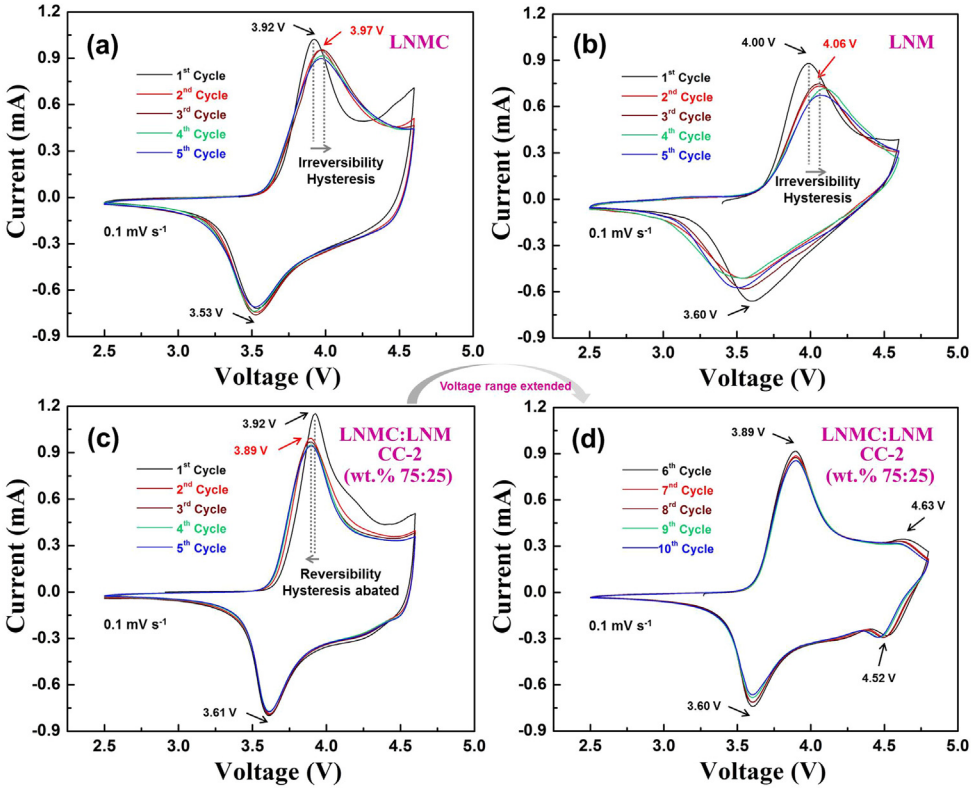

Fig. 5. Cyclic voltammograms of (a) Li *vs* LNMC, (b) Li *vs* LNM and (c) Li *vs* CC-2 cell in the voltage range from 2.5 to 4.6 V (1st–5th cycles) and (d) Li *vs* CC-2 cell voltage range extended to 4.8 V (6th–10th cycles) at 0.1 mV s^{-1} (1 M $LiPF_6$ in 1:1 EC–DMC solvents). In the CV scans, irreversibility and reversibility (hysteresis, hysteresis free) are indicated using arrows (→/←).

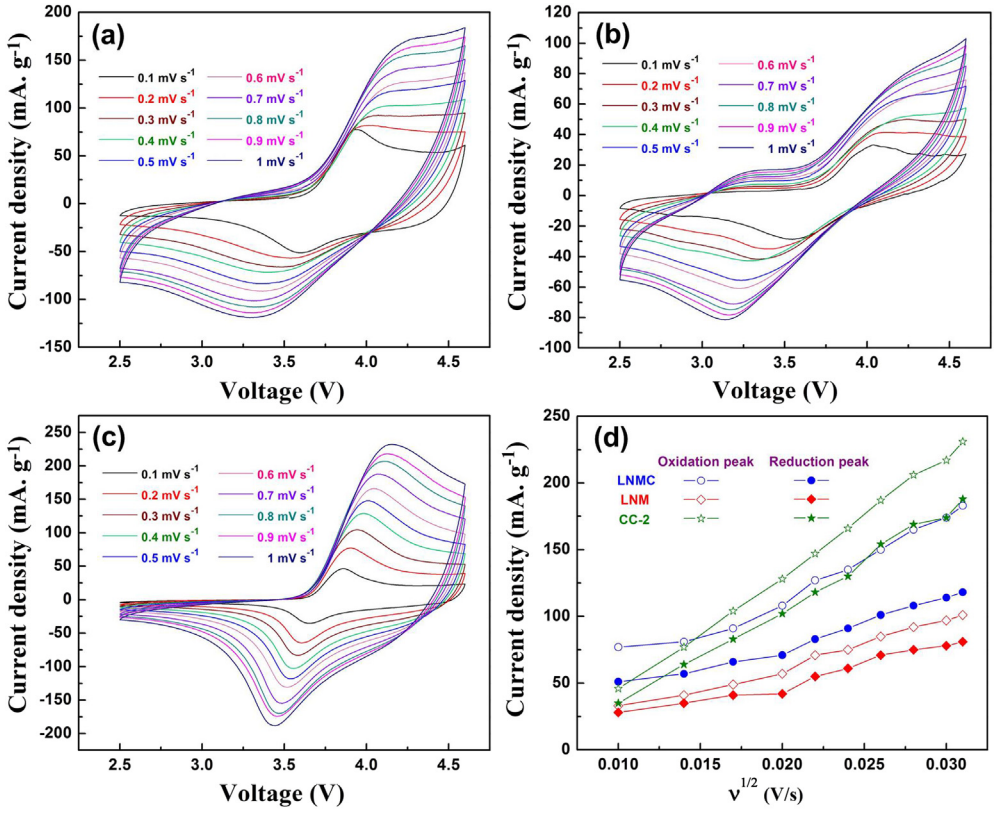

Fig. 6. Cyclic voltammograms @ 0.1–1 mV s^{-1} for cells: (a) Li *vs* LNMC, (b) Li *vs* LNM and (c) Li *vs* CC-2 in the voltage range from 2.5 to 4.6 V and (d) the corresponding current density *vs* scan rate ($\upsilon^{1/2}$).

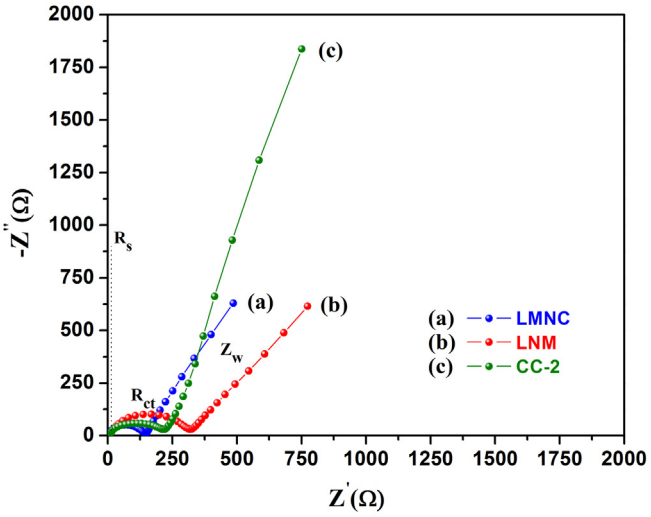

Fig. 7. Electrochemical impedance spectra of (a) Li *vs* LNMC, (b) Li *vs* LNM and (c) Li *vs* CC-2 cell in the frequency range of 100 kHz to 10 mHz (1 M $LiPF_6$ in 1:1 EC–DMC solvents).

3.4. $\Delta\varphi_p$ potential difference of cathode phase/material through CV investigation

Clear insight on oxidation–reduction based electrochemical reaction obtained using CV studies holds the key for explaining the electrochemical performance of the battery system. Accordingly, Fig. 5 depicts the CV profile of different (LNMC, LNM and CC-2) cathode phase/material *versus* Li at 0.1 mV s^{-1}. CV scans (in the range 2.5–4.6 V) representing anodic-oxidation/cathodic-reduction peaks occur respectively at 3.92/3.53 V (LNMC, Fig. 5a), 4.00/3.60 V (LNM, Fig. 5b) and 3.92/3.61 V (CC-2, Fig. 5c) corresponding to the Ni^{2+}/Ni^{4+} redox process for these cathode phase/material. The prominent high voltage hump occurring at 4.6 V for the LNMC and CC-2 composite cathode material could be attributed to Co^{3+}/Co^{4+} redox process in line with similar observation reported for LNMC earlier [41]. Also it is significant to note that there is no redox peak around 3 V region implying the absence of Mn ions in the 3+ state [42]. Describing the details of the 1st scan: it is known that the difference $\Delta\varphi_p$ between anodic peak potential φ_{pa} and cathodic peak potential φ_{pc} can be the measure of the reversibility of the intercalation process [43]. This difference ($\Delta\varphi_p$) found to be showing low values of 0.39 V (LNMC), 0.40 V (LNM) and 0.31 V (CC-2) as against a nominal limit of 0.5 V indicating good reversibility of the redox processes for these layered samples. Comparing $\Delta\varphi_p$ values, we have that the CC-2 phase shows the least value of 0.31 V which might suggest superior reversibility of the Li^+ intercalation process. In the second scan, the LNMC/LNM phases exhibit a small higher voltage shift (3.92 V–3.97 V/4.00–4.06 V, Fig. 5a, b) in the major anodic peak whilst for the CC-2 material reverse happens that is the anodic peak shift towards lower voltage (3.92 V–3.89 V, Fig. 5c). For all the samples subsequent CV scans almost traced the profile of 2nd scan indicating good reversibility. Impressively a small $\Delta\varphi_p$ values 0.28 V (2nd scan) obtained for the CC-2 material indicates a good reversibility of the Li^+ intercalation process which might eventually enhance the electrochemical performance. The initial CV profile difference observed in the anodic peak can be rationalized by considering active electrolyte

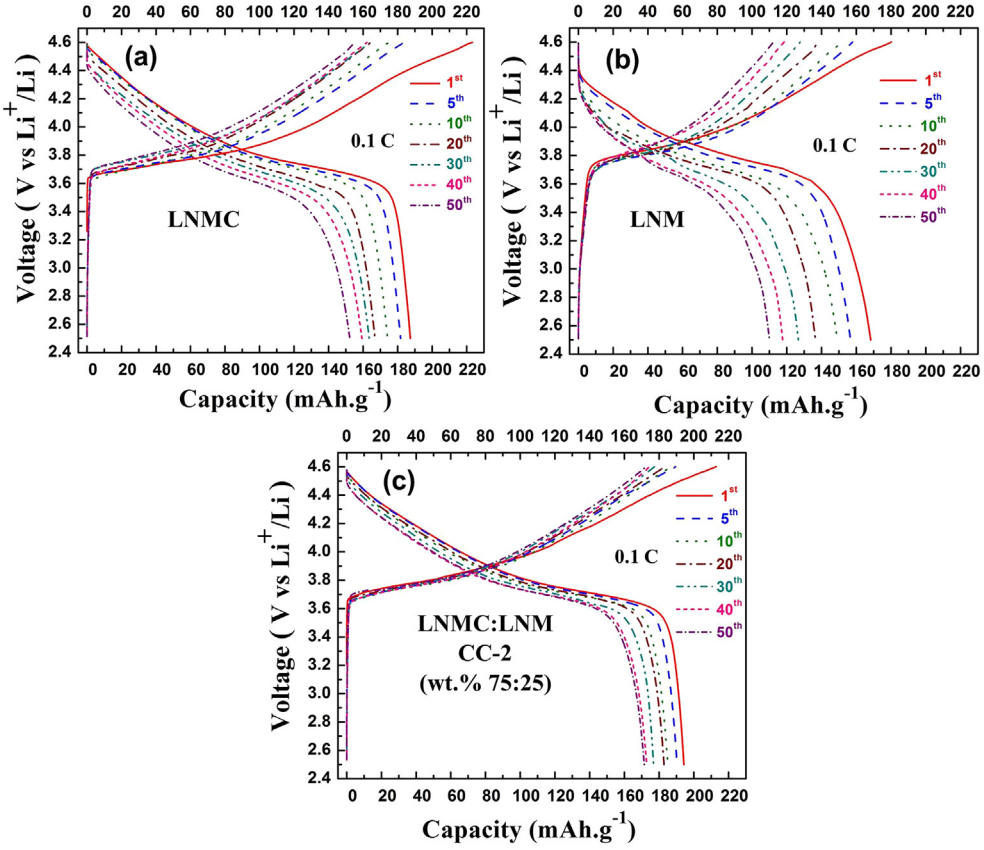

Fig. 8. Charge–discharge studies on individual and composite cathode phase/materials: voltage *vs* capacity profile of (a) Li *vs* LNMC, (b) Li *vs* LNM and (c) Li *vs* CC-2 cell in the voltage range from 2.5 to 4.6 V at 0.1 C (1 M $LiPF_6$ in 1:1 EC–DMC solvents).

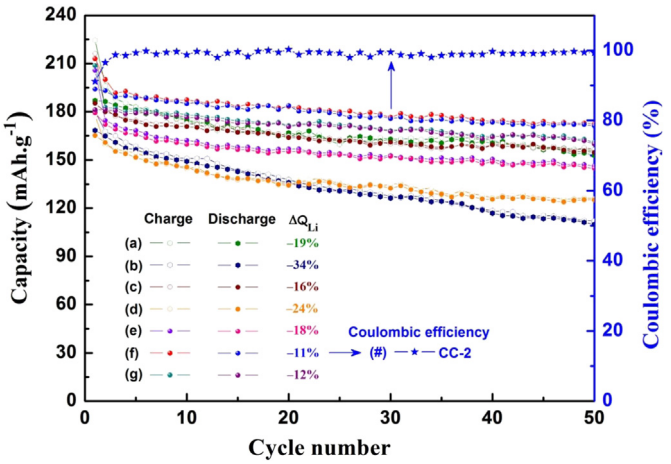

Fig. 9. Charge–discharge studies on as-prepared, milled and composite cathode phase/materials: capacity *vs* cycle number performance of (a) Li *vs* LNMC, (b) Li *vs* LNM, (c) Li *vs* LNMC-milled, (d) Li *vs* LNM-milled, (e) Li *vs* CC-1, (f) Li *vs* CC-2 and (g) Li *vs* CC-3 cells in the voltage range from 2.5 to 4.6 V at 0.1 C. Discharge capacity drop ΔQ_{Li} (negative sign indicating capacity decrease upon cycling) indicated in respective cases of cathode phase/materials. Corresponding coulombic efficiency data for the optimized composite cathode CC-2 phase also indicated.

decomposition and passive film formation processes. In view of the impressive CV behavior of the CC-2 composite cathode, the scope of the CV studies on the cell has been further extended to 4.8 V (6th–10th cycles) as depicted in Fig. 5d. These scans yielded pronounced two oxidation peaks located at 3.89 and 4.63 V, while the reduction peaks observed at 3.6 and 4.52 V, correspond to the Ni^{2+}/Ni^{4+} and Co^{3+}/Co^{4+} redox processes with a marked decrease of current [44]. This current change can be explained through change of the lattice dimensions of CC-2 exhibiting only a small decrease in lattice parameters [45] or a drastic decrease in unit-cell volume [46]. In addition, it can also be explained by considering the deeply delithiated electrode losing their structural stability and hence the reversibility of Li^+ intercalation [47]. Summing up of results of the CV studies, we have that barring the initial cycle there is perfect overlap of CV traces of CC-2 composite cathodic phase from 1st–5th cycle (2.5–4.6 V) indicating excellent reversibility for (de) intercalation of Li species (Fig. 5c) [41]. Detailed CV studies with scan rates (0.1–1 mV s^{-1}) *versus* current densities (mA g^{-1}) have been carried out (Fig. 6a–c). It is found that the value of diffusion coefficient deduced (Fig. 6d) for the optimized composite cathode phase CC-2 essentially follow that of the constituents LNMC phase which is in the range of 10^{-6} being one order higher than the other LNM phase (10^{-7}).

In order to have clear information on localization and mobility of charges (having frequency dependence) EIS studies have been carried out for (a) Li *vs* LNMC, (b) Li *vs* LNM and (c) Li *vs* CC-2 cells as depicted in Fig. 7. From this EIS results, we have that the cell made with CC-2 cathode stands apart in terms of pronounced Warburg profile characterizing a dominant diffusion process which is good agreement with CV results.

Table 2
Comparison of electrochemical performance of cathode phase/material *viz.*, LNMC, LNM, LNMC-milled, LNM-milled, CC-1, CC-2 and CC-3.

Sample	Initial charge/discharge capacity (mAh g^{-1})	Capacity loss (mAh g^{-1})	Columbic efficiency (%)	Discharge capacity drop ΔQ_{Li} (%)
LNMC	224/187	37	83	−19
LNM	180/168	12	93	−34
LNMC-milled	216/185	31	85	−16
LNM-milled	177/165	12	93	−24
CC-1	205/179	26	87	−18
CC-2	213/194	19	91	−11
CC-3	208/181	27	87	−12

3.5. Capacity retention of cathode phase/material through charge–discharge studies

Galvanostatic charge–discharge study constitutes the most important step in evaluating the performance and feasibility of any electrochemical system fabricated for useful application. Accordingly, results of charge–discharge studies made for the electrochemical cell using LNMC, LNM and CC-2 cathode phase/material under 0.1 C rate, 2.5–4.6 V range upto 50 cycles are presented in Fig. 8a–c and Fig. 9. From the voltage profile, it is possible to infer the presence of one main voltage plateau occurring in the region ~4 V for the cell using LNMC (Fig. 8a), LNM (Fig. 8b) and CC-2 (Fig. 8c) cathode phase/material. The initial charge–discharge capacity of the LNMC, LNM, LNMC-milled, LNM-milled, CC-1, CC-2 and CC-3 composite cathode materials were found to be 224/187 mAh g^{-1}, 180/168 mAh g^{-1}, 216/185 mAh g^{-1}, 177/165 mAh g^{-1}, 205/179 mAh g^{-1}, 213/194 mAh g^{-1} and 208/181 mAh g^{-1}. In spite of the large irreversible capacity of the individual LNMC (37 mAh g^{-1}) and LNM phases (12 mAh g^{-1}), the CC-2 composite

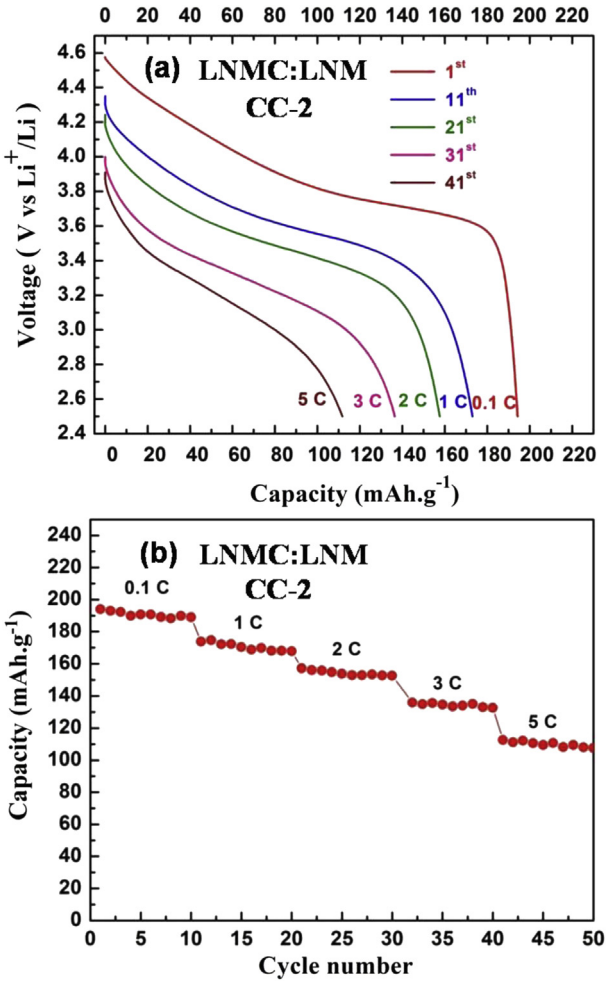

Fig. 10. Rate capability studies on the composite cathode material (a) voltage *vs* capacity profile and (b) capacity *vs* cycle number performance for the Li *vs* CC-2 cell at different rates: 0.1 C, 1 C, 2 C, 3 C, 5 C.

cathode material delivered high discharge capacity of 194 mAh g^{-1} with minimized irreversible capacity of 19 mAh g^{-1} in the voltage range 2.5–4.6 V for the 1st cycle. Also it can be seen that voltage drop and polarization of CC-2 composite material at 50th cycle was less and the resulting discharge voltage profile stabilizing at 4.5 V than 4.4 V (LNMC) and 4.2 V (LNM) for the same 50th cycle as depicted in Fig. 8a–c. Turning to discuss the galvanostatic cycling performance of these cathode phase/material (Fig. 9), it is observed that the Li *vs* LNMC cell exhibited gradual capacity fading upon cycling and the capacity retention was about 82% for 50 cycles. Also, the Li *vs* LNM cell indicates 65% capacity retention with pronounced capacity fading for 50th cycle. Moving to the composite cathode phase, the Li *vs* CC-2 cell showed good capacity retention, maintaining ~88% of its initial capacity during the 50th cycle. The charge–discharge capacities of CC-2 composite cathode materials at 1st and 50th cycles are 213/194 mAh g^{-1} and 172/171 mAh g^{-1} respectively. The capacity fade upon cycling is small (@0.8 mAh g^{-1} per cycle during the first five cycles), which progressively decreased further impressively upon cycling (@0.2 mA per cycle at 46th–50th cycles). Careful scrutiny of the data given in Table 2 in conjunction with the capacity *vs* cycle number profile depicted in Fig. 9, we have that cycle capacity of the composite cathode material is higher than LNMC notwithstanding initial higher capacity of the latter upon charging. This can be rationalized in terms of pronounced capacity fade observed for the LNM phase resulting in much lower capacity at 50th cycle. Furthermore, for the composite cathode material precise control on discharge capacity drop ΔQ_{Li} (−11%, negative sign indicating a decrease) becomes possible while for the constituent LNMC/LNM phase, the capacity drop values are nearly two/three fold higher (−19% for LNMC, −34% for LNM). Corresponding coulombic efficiency data for the optimized composite cathode CC-2 phase has also been indicated (Fig. 9, Table 2).

Inherent capacity fading present in this system of material can be correlated with progressively increasing surface passivation on CC-2 electrode entailing in ohmic drop upon prolonged cycling. Turning to explain the mechanism of capacity fading: it is possible that the important cause could be the dissolution of CC-2 active material in the electrolyte during cycling which can be attributed to the existence of HF easily formed through $LiPF_6$ used as the electrolyte salt [48,49]. The charge–discharge results of the present investigation are found to be comparable to the capacity fade reported earlier for the layered LNMC materials [44]. Rate capability studies, voltage *vs* capacity profile (Fig. 10a) and capacity *vs* cycle number performance (Fig. 10b) indicate that CC-2 composite cathode material delivers high discharge capacities under different rates: 194 mAh g^{-1} (0.1 C), 173 mAh g^{-1} (1 C), 157 mAh g^{-1} (2 C), 135 mAh g^{-1} (3 C) and 112 mAh g^{-1} (5 C). Also, it can be generalized that at higher rates, there is a considerable drop in capacity values together with a drop in discharge voltage plateau which may be caused by high electrode polarization as depicted in Fig. 10a.

3.6. Smooth surface of cathode particles abates capacity hysteresis

In the design of batteries for gainful applications several key parameters *viz.*, cell voltage, capacity and more important the safety issue have to be taken in to consideration [23]. Although, the first two parameters can easily be met through the judicious choice of battery components in particular the cathode system, it is a daunting task to address the last criterion. This motivated Li-ion battery community to scurry for improving the battery design. Preparing composite cathode material of layered LNMC and LNM systems is an effective strategy for addressing the safety issue without compromising capacity [23]. In the course of making composite cathode material which essentially involves blending of two individual phases through gentle milling, particles of the resultant composite cathode material gets reasonably smoothened in comparison to edged particles of the individual phases.

In terms of transportation of charges (both Li^+ and e^-) through intercalation, potential difference there is drastic difference in the behavior between edges and smooth surface of cathode particle

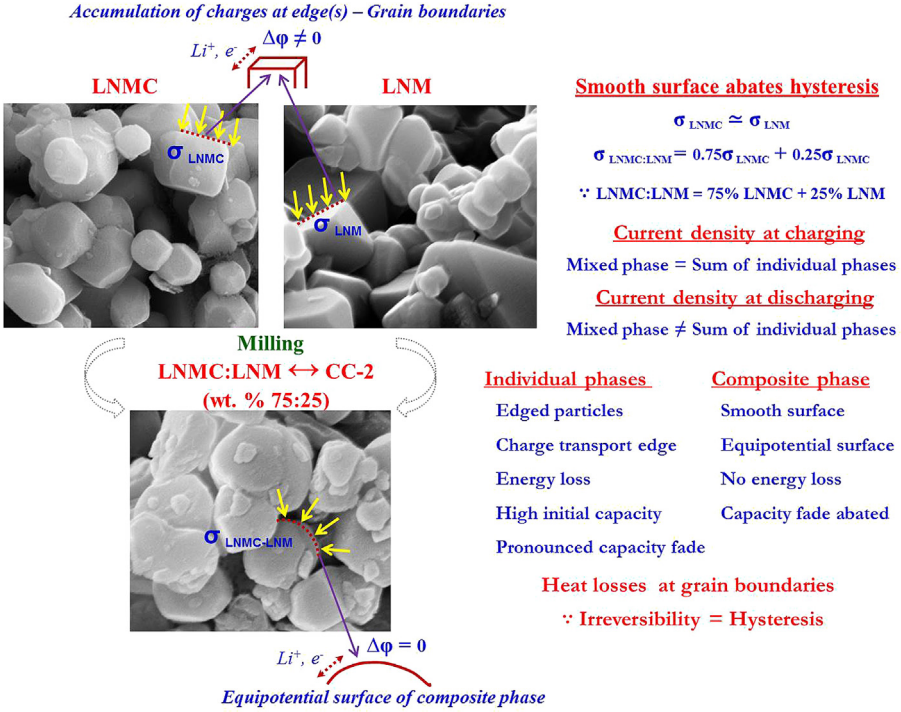

Fig. 11. Schematics illustrating concentration, transportation of charges (Li^+, e^-) across the edges of faceted particles of individual cathodic phase(s) *vs* moving over smooth particle surface of the composite cathodic phase.

[10,50]. That is the former exhibits pronounced propensity to accumulate charges [10] while the latter tends towards a near equipotential surface. This means that little work (energy) needs to be done in moving a charge over a smooth surface ($\Delta\varphi = 0$) in contrast to sharp edges necessitating much work ($\Delta\varphi \neq 0$) for the itinerant charges. To describe the exact scenario, the complexion of shuttling of charges across edges of the cathode particles involves multiple processes such as charge transportation, switching between edge ↔ face of the cathode particles and energy loss etc., Under charging condition, the charge capacity of the composite cathode particle is nearly the same as that of individual phases (75% + 25%, Fig. 9, Table 2). This can be rationalized in terms of almost equal charge densities as indicated from same capacity of the constituent individual phases (σ_{LNMC}, σ_{LNM}) making up the charge density of the composite cathode material ($\sigma_{LNMC:LNM}$) particles through the linear sum of the current densities of constituent phases (relative weight) having little scope for losing charges during charging as illustrated in Fig. 11. On the other hand, during discharging the process acquires more complex picture arising from multiple processes because itinerant charges need to encounter transport across two dissimilar surfaces, thermal loss etc., Importantly shuttling a charge between surfaces of different curvatures stemming from grain boundaries due to edges definitely entails in potential barrier eventually costing the free energy of the system which in turn manifests in decreased capacity thus accounting pronounced capacity loss for the individual phases. Quite advantageously these short-comings are overcome in the smoothened surface of the composite cathode particles offering no such losses accounting for impressive capacity performance. Indeed the corresponding CV profiles (Fig. 5a, b) has corroborated the occurrence of such losses as reflected from the shift towards higher voltage suggesting irreversibility hence grain boundary-edge induced hysteresis for the individual phases. Not fortuitously, the composite cathode material showed abated hysteresis facilitating good capacity retention as a result of potential shift towards lower voltage indicating high reversibility (Fig. 5c).

In this context, it is pertinent to take note of pioneering work of S. Hang et al., highlighting importance of grain boundaries of cathode particles in influencing Li-ion diffusivity eventually determining the capacity [51]. From this, we have that expression (3) for the current density (J_{gb}) given by

$$J_{gb} = -D_{gb}\nabla C_{gb}(n, t_1, t_2, t) \quad (3)$$

with D_{gb}, ∇C_{gb}(n, t_1, t_2, t) respectively being grain boundary diffusion coefficient and concentration gradient. By virtue of accumulation charges along the edges (grain-boundaries) the value of D_{gb} is bound to be much greater than the diffusion coefficient charges at the core of the particles (D_g) eventually leading to anisotropy in charge concentration gradient. This might give large scope for irreversible capacity-hysteresis upon discharge. Whilst in the composite cathode material comprising smooth particles, this kind of anisotropy is not expected to occur which might be useful to account for high capacity with good capacity retention observed.

3.7. Graphitic alloy anode charge–discharge studies

Presently, graphitic anode when used in the battery application has some drawbacks such as limited capacity and safety issue. Particularly, the chemical instability arising from the formation of solid electrolyte interface (SEI) layer through the reaction of carbon anode surface with the electrolyte and the lithium plating on the SEI layer owing to a charge–discharge potential close to that of Li/Li^+. These difficulties generated large interest in the development of alternative anode materials for Li-ion batteries [52]. Accordingly, much effort has been directed towards the development of new electrode systems capable of exploiting potential of nanostructure materials devoted to electrochemistry [53]. Notably, the active/inactive nano composite concept has been particularly developed [54]. The working concept of this system underlies the mixture of two or more materials, one electrochemically reacting with lithium while the other acts as an electrochemically inactive confining buffer to accommodate the large volume changes accompanying the electrochemical process [55]. Sony has introduced such a new Li-ion battery system with new concept alloy anode material [56].

Electrochemical performance of the graphitic anode can be considerably improved through alloying with other metal powders such as Sn, Ti and Ni as illustrated in Fig. 12. Describing the results in detail we have that the cell made using commercial graphite powder yielded a moderate capacity of ~200 mAh g^{-1} while alloying with Sn powder delivered an enhanced capacity of ~280 mAh g^{-1} with drastic undesirable capacity fade. But significant abatement in capacity fade became feasible with the introduction of Ti and Ni species. In particular the alloy composition corresponding to $G_{0.65}Ni_{0.05}Ti_{0.15}Sn_{0.15}$ yielded remarkable capacity coupled with good capacity retention results (Fig. 12). Discharge–charge voltage profile obtained for the Li *vs* $G_{0.65}Ni_{0.05}Ti_{0.15}Sn_{0.15}$ cell at a constant current density of 37 mA g^{-1} is given in Fig. 12a. Cycling performance of different alloy anode materials with

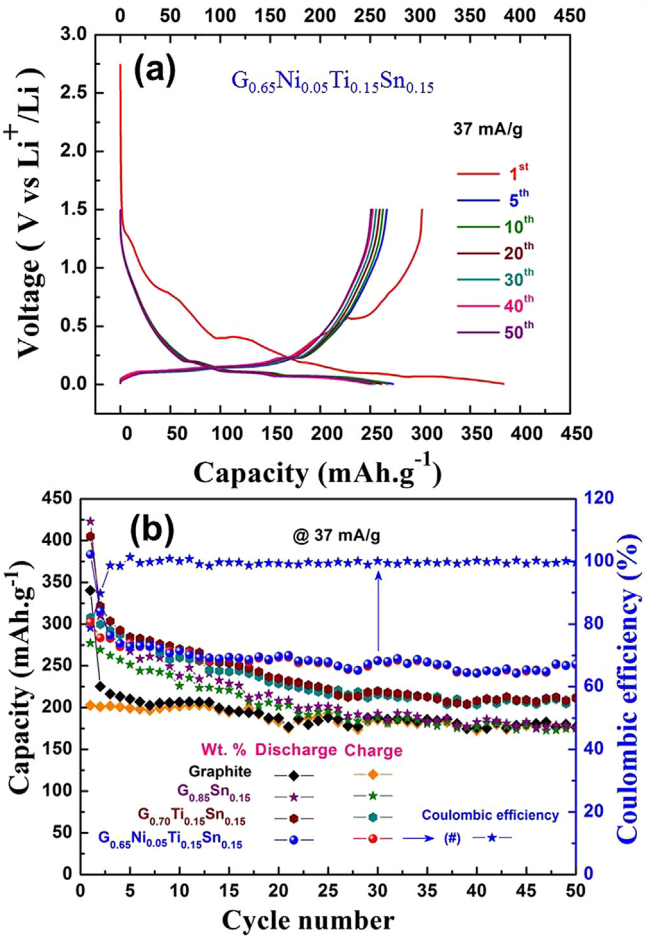

Fig. 12. Discharge–charge studies on graphitic alloy anode: (a) voltage *vs* capacity profile and (b) capacity *vs* cycle number performance in the voltage range from 0.005 to 1.5 V at 37 mA g^{-1} (1 M $LiPF_6$ in 1:1 EC–DMC solvents). Corresponding coulombic efficiency data for the optimized composite anode also indicated.

compositions (in wt. %) graphite, $G_{0.85}Sn_{0.15}$, $G_{0.70}Ti_{0.15}Sn_{0.15}$ and $G_{0.65}Ni_{0.05}Ti_{0.15}Sn_{0.15}$ at constant current of 37 mA g^{-1} are depicted in Fig. 12b. From this, Li *vs* $G_{0.65}Ni_{0.05}Ti_{0.15}Sn_{0.15}$ cell delivered the highest capacity coupled with impressive capacity retention during cycling (1–50 cycle). Cycle performance details of the high performance $G_{0.65}Ni_{0.05}Ti_{0.15}Sn_{0.15}$ alloy anode being: the initial discharge/charge capacity (383/302 mAh g^{-1}) showed large irreversible capacity 81 mAh g^{-1} (~21%). But this drop could be completely abated in the second cycle onwards (discharge/charge capacity, 315/283 mAh g^{-1}) the irreversible capacity is reduced to 32 mAh g^{-1} (10%). To rationalize the pronounced drop observed during the starting of the lithiation process in the 1st cycle, traces of oxides of the alloying metals present get converted to metal and Li_2O leading to irreversible capacity because Li cannot be extracted from Li_2O during the electrochemistry reaction [57]. Also, the formation of SEI film on the electrode surface may facilitate high initial capacity of alloy anode [58]. After the second cycle, Li cell with $G_{0.65}Ni_{0.05}Ti_{0.15}Sn_{0.15}$ alloy anode delivered stable capacity of ~265 mAh g^{-1} with excellent cyclability over 50 cycles.

3.8. Li-ion pouch cell: features and performance

In view of several advantages of Li-ion pouch cell such as light weight, low cost, high energy density it is most preferred for electric vehicle applications over other type of Li-ion cells [59]. Electrochemical studies on this type of high energy storage Li-ion pouch cell ($G_{0.65}Ni_{0.05}Ti_{0.15}Sn_{0.15}$ *vs* CC-2) fabricated in our lab delivered a cell capacity of ~500 mAh. After an aging of 24 h, this cell was used for further electrochemical studies. Turning to the electrochemical performance of Li-ion pouch cell, it is essential to pass through the formation cycle comprising charging in two continuous steps *viz.*, constant current (CC) mode at 15 mA upto 4.6 V (low current) and constant voltage (CV) mode with drawn current allowing only 5% rated capacity of the cell [60]. The performance of cell capacity *vs* cycles (0.1 C, 50 mA) for the Li-ion pouch cell is shown in Fig. 13a. The formation cycle is the essential step for stabilization of active materials through SEI film formation in the cell [60,61]. Formation of SEI film over the anode has the intrinsic advantage of preventing further chemical reaction between electrolyte and active materials. It is expected that the low current (15 mA) applied can produce a dense SEI layer which is advantageous for improving cyclability of the Li-ion pouch cell. Extending our investigations to evaluate cell capacity and cycling performance of the Li-ion pouch cell in the voltage range 2.5–4.6 V up to 100 cycles (0.1 C, 50 mA) are given in Fig. 13a. In particular, thus fabricated Li-ion pouch cell delivered a discharge capacity of ~500 mAh at 15th cycle in the voltage range 2.5–4.6 V. Furthermore, the capacity fade is similar to Li *vs* CC-2 cell which can be explained along the same lines as discussed for cathode earlier. Because the fabricated Li-ion pouch cell had to be use in demonstration cycles studies were limited to 100 cycles. After 100 cycles of charge–discharging the open circuit voltage measured was found to be 4.41 V (Fig. 13b). In order to demonstrate the utility of the Li-ion pouch cell in real applications it was used for energizing 40 LEDs (load = 0.12 Wh, ~15 h/charge, Fig. 13c) and also running a toy-car with a load 1.1 Wh on a smooth flooring tiles (Fig. 13d) at CSIR-CECRI (video demonstration for Li-ion pouch cell in supplementary S1). During this demonstration, illuminating the 40 LEDs consumed a current of 35 mA while running of the toy-car consumed current at the rate of 315 mA. This amply vouches for its application in futuristic energy storage systems.

Supplementary video related to this article can be found at http://dx.doi.org/10.1016/j.jpowsour.2014.04.064.

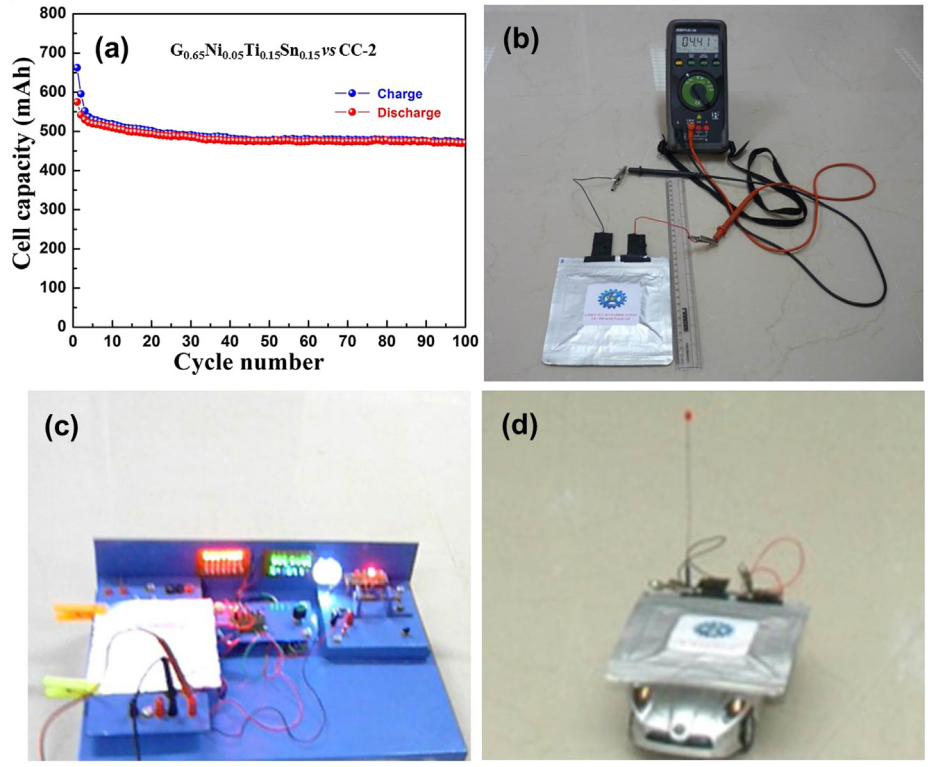

Fig. 13. Li-ion pouch cell features and performance: (a) cell capacity *vs* cycle number in the voltage range from 2.5 to 4.6 V up to 100 cycles (1 M $LiPF_6$ in 1:1 EC–DMC solvents); (b) photograph illustrating the open circuit voltage (4.41 V) after 100 cycles at charge condition; fabricated Li-ion pouch cell (500 mAh) in action used (c) to illuminate 40 LEDs for lighting and (d) to energize toy-car running on tiled floor at CSIR-CECRI, India.

4. Conclusion

Considering the important safety aspect of the Li-ion batteries for applications, the CC-2 composite cathode material (wt. % 75:25) has been obtained through a gentle milling of well characterized LNMC and LNM phases synthesized using facile thermolysis employing MHC precursor. This composite cathode material expectedly delivered impressive charge–discharge features *viz*., 194 mAh g^{-1} (0.1 C), 173 mAh g^{-1} (1 C), 157 mAh g^{-1} (2 C), 135 mAh g^{-1} (3 C) and 112 mAh g^{-1} (5 C) in the voltage range 2.5–4.6 V. Although the charge–discharge capacity of the individual phases *viz*., LNMC, LNM showed an impressive value of 224/187; 180/168 mAh g^{-1} attributed to sharp edges of the cathode particles, these individual phases showed pronounced irreversible capacity-hysteresis. Upon discharging of the composite phase, irreversible capacity of the system is found to be absent which can be attributed to milled/smoothened cathode particles of the composite phase. Also there is significant control on fade for the milled particles of the constituent cathode phases. Hence, it seems reasonable to hypothesize that edge-free cathode particles providing a near isotropic equipotential surface for the hassle free transport of charges facilitating abatement of irreversible capacity-hysteresis of the composite cathode material so as to be useful for gainful applications. The design potential of the high performance composite cathode material could be extended with the fabrication of Li-ion pouch cell (~500 mAh, W-weaving style) in conjunction with the use of graphitic alloy anode ($G_{0.65}Ni_{0.05}Ti_{0.15}Sn_{0.15}$) material under moderate loads 0.12 Wh, 1.1 Wh during demonstration.

Acknowledgment

The first author, P. Manikandan, acknowledges the Council of Scientific and Industrial Research (CSIR), New Delhi for granting the financial support for the above work in the form of a senior research fellowship and also our thanks to the Director, CSIR-CECRI, Karaikudi.

References

[1] M. Armand, J.M. Tarascon, Nature 451 (2008) 652–657.
[2] A. Armstrong, P. Bruce, Nature 381 (1996) 499–500.
[3] J. Tarascon, M. Armand, Nature 414 (2001) 359–367.
[4] M. Whittingham, Chem. Rev. 104 (2004) 4271–4301.
[5] J.N. Reimers, J.R. Dahn, J. Electrochem. Soc. 139 (1992) 2091–2097.
[6] Z. Lu, D.D. MacNeil, J.R. Dahn, Electrochem. Solid-State Lett. 4 (2001) A200–A203.
[7] D. MacNeil, Z. Lu, J.R. Dahn, J. Electrochem. Soc. 149 (2002) A1332–A1336.
[8] Y.K. Sun, S.T. Myung, H.J. Bang, B.C. Park, S.J. Park, N.Y. Sung, J. Electrochem. Soc. 154 (2007) A937–A942.
[9] T. Ohzuku, Y. Makimura, Chem. Lett. 30 (2001) 642–643.
[10] P. Manikandan, P. Periasamy, R. Jagannathan, J. Power Sources 245 (2014) 501–509.
[11] K. Kang, Y.S. Meng, J. Bréger, C.P. Grey, G. Ceder, Science 311 (2006) 977–980.
[12] P. Manikandan, M.V. Ananth, T. Prem Kumar, M. Raju, P. Periasamy, K. Manimaran, J. Power Sources 196 (2011) 10148–10155.
[13] Z. Wang, Y. Sun, L. Chen, X. Huang, J. Electrochem. Soc. 151 (2004) A914–A921.
[14] T. Ohzuku, Y. Makimura, Chem. Lett. 30 (2001) 744–745.
[15] X. Luo, X. Wang, L. Liao, S. Gamboa, P.J. Sebastian, J. Power Sources 158 (2006) 654–658.
[16] Z. Lu, D.D. MacNeil, J.R. Dahn, Electrochem. Solid-State Lett. 4 (2001) A191–A194.
[17] Z. Lu, L.Y. Beaulieu, R.A. Donaberger, C.L. Thomas, J.R. Dahn, J. Electrochem. Soc. 149 (2002) A778–A791.
[18] S.K. Martha, H. Sclar, Z.S. Framowitz, D. Kovacheva, N. Saliyski, Y. Gofer, P. Sharon, E. Golik, B. Markovsky, D. Aurbach, J. Power Sources 189 (2009) 248–255.
[19] P. Periasamy, N. Kalaiselvi, J. Power Sources 159 (2006) 1360–1364.
[20] P. Gao, G. Yang, H. Liu, L. Wang, H. Zhou, Solid State Ionics 207 (2012) 50–56.
[21] E.L. Uzunova, I.G. Mitov, G. Klissurski, J. Mater. Chem. 6 (1996) 1035–1040.
[22] K.W. Nam, W.S. Yoon, H. Shin, K.Y. Chung, S. Choi, X.Q. Yang, J. Power Sources 192 (2009) 652–659.
[23] K.S. Lee, S.T. Myung, Y.K. Sun, J. Power Sources 195 (2010) 6043–6048.
[24] B.C. Park, H.J. Bang, K. Amine, E. Jung, Y.K. Sun, J. Power Sources 174 (2007) 658–662.
[25] T. Numata, C. Amemiya, T. Kumeuchi, M. Shirakara, M. Yonezawa, J. Power Sources 97–98 (2001) 358–360.
[26] Z.F. Ma, X.Q. Yang, X. Sun, J. McBreen, J. New Mater. Electrochem. Syst. 4 (2001) 121–125.
[27] Z.F. Ma, X.Q. Yang, X.Z. Liao, X. Sun, J. McBreen, Electrochem. Commun. 3 (2001) 425–428.
[28] H. Kitao, T. Fujihara, K. Takeda, N. Nakanishi, T. Nohma, Electrochem. Solid-State Lett. 8 (2005) A87–A90.
[29] S.T. Myung, M.H. Cho, H.T. Hong, T.H. Kang, C.S. Kim, J. Power Sources 146 (2005) 222–225.
[30] J. Yang, X. Zhang, X. Han, F. Cheng, Z. Tao, J. Chen, J. Mater. Chem. A 1 (2013) 13742–13745.
[31] J.F. Whitacre, K. Zaghib, W.C. West, B.V. Ratnakumar, J. Power Sources 177 (2008) 528–536.
[32] J. Baker, M. Saudi, K. Yazid, E. Tracy, US Patent 7, 041, 2006, 239.
[33] M. Uno, K. Ogawa, Y. Takeda, Y. Sone, K. Tanaka, M. Mita, H. Saito, J. Power Sources 196 (2011) 8755–8763.
[34] Y. Fujii, H. Miura, N. Suzuki, T. Shoji, N. Nakayama, J. Power Sources 171 (2007) 894–903.
[35] X. Luo, X. Wang, L. Lao, X. Wang, S. Gamboa, P.J. Sebastian, J. Power Sources 161 (2006) 601–605.
[36] J.N. Reimers, E. Rossen, C.D. Jones, J.R. Dahn, Solid State Ionics 61 (1993) 335–344.
[37] X. Wu, X. Li, Z. Wang, H. Guo, P. Yue, Y. Zhang, Appl. Surf. Sci. 268 (2013) 349–354.
[38] K. Nakamoto, Infrared and Raman Spectra of Inorganic and Coordination Compounds Part A: Theory and Applications in Inorganic chemistry, fifth ed., John Wiley & Sons, 1997.
[39] N.V. Kosova, E.T. Devyatkina, V.V. Kaichev, J. Power Sources 174 (2007) 965–969.
[40] L.A. Riley, S.V. Atta, A.S. Cavanagh, Y. Yan, S.M. George, P. Liu, A.C. Dillon, S.H. Lee, J. Power Sources 196 (2011) 3317–3324.
[41] F. Wu, M. Wang, Y. Su, L. Bao, S. Chen, J. Power Sources 195 (2010) 2362–2367.
[42] Y.S. He, Z.F. Ma, X.Z. Liao, Y. Jiang, J. Power Sources 163 (2007) 1053–1058.
[43] B. Zhang, G. Chen, P. Xu, C.C. Li, J. Power Sources 176 (2008) 325–331.
[44] Y.J. Shin, W.J. Choi, Y.S. Hong, S. Yoon, K.S. Ryu, S.H. Chang, Solid State Ionics 177 (2006) 515–521.
[45] D.C. Li, T. Muta, L.A. Zhang, M. Yoshio, H. Noguchi, J. Power Sources 132 (2004) 150–155.
[46] N. Yabuuch, T. Ohzuku, J. Power Sources 119–121 (2003) 171–174.
[47] A. Rougier, P. Gravereau, C. Delmas, J. Electrochem. Soc. 143 (1996) 1168–1175.
[48] H.F. Xiang, H. Wang, C.H. Chen, X.W. Ge, S. Guo, J.H. Sun, W.Q. Hu, J. Power Sources 191 (2009) 575–581.
[49] S.F. Lux, I.T. Lucas, E. Pollak, S. Passerini, M. Winter, R. Kostecki, Electrochem. Commun. 14 (2012) 47–50.
[50] X. Zhang, A.M. Sastry, W. Shyy, J. Electrochem. Soc. 155 (2008) A542–A552.
[51] S. Han, J. Park, W. Lu, A.M. Sastry, J. Power Sources 240 (2013) 155–167.
[52] R.A. Huggins, Solid State Ionics 113 (1998) 57–67.
[53] A.S. Arico, P. Bruce, B. Scrosati, J.M. Tarascon, W.V. Schalkwijk, Nat. Mater. 4 (2005) 366–377.
[54] M. Winter, J.O. Besenhard, Electrochimica Acta 45 (1999) 31–50.
[55] R.A. Huggins, in: G.-A. Nazri, G. Pistoia (Eds.), Lithium Batteries, Kluwer Academic, Boston, 2004.
[56] S. Kawakami, M. Asao, US Patent No: 6949312, 2005.
[57] S. Ohara, J. Suzuki, K. Sekine, T. Takamura, J. Power Sources 136 (2004) 303–306.
[58] H. Li, X.J. Huang, L.Q. Chen, Z.G. Wu, Y. Liang, Electrochem. Solid-State Lett. 2 (1999) 547–549.
[59] K. Amine, I. Belharouak, Z. Chen, T. tran, H. Yummoto, N. Ota, S.T. Myung, Y.K. Sun, Adv. Mater. 22 (2010) 3052–3057.
[60] S.S. Zhang, J. Power Sources 161 (2006) 1385–1391.
[61] H.H. Lee, Y.Y. Wang, C.C. Wan, M.H. Yang, H.C. Wu, D.T. Shieh, J. Power Sources 134 (2004) 118–123.